Powder Technology 286 (2015) 371–377

Contents lists available at ScienceDirect

Powder Technology

journal homepage: www.elsevier.com/locate/powtec

Study of Co and Fe-doped ZnO milled nanopowders

M. Meyer *, L.C. Damonte

Facultad de Ciencias Exactas, Departamento de Física, Universidad Nacional de La Plata (UNLP), CC 67, 1900 La Plata, Argentina
Instituto de Física La Plata (IFLP, CONICET), La Plata, Argentina

ARTICLE INFO

Article history:
Received 11 March 2015
Received in revised form 20 May 2015
Accepted 2 July 2015
Available online 9 July 2015

Keywords:
Semiconductors
Nanoparticle
XAFS

ABSTRACT

Fe and Co-doped ZnO powders obtained by mechanical milling from different starting materials are presented. Both the local structural and the magnetic properties are investigated using X-ray diffraction, XAFS and magnetic measurements. The evolution of these properties with milling time, atomic content and milling atmosphere is analyzed. XAFS measurements revealed the progressive incorporation of doped atoms into the ZnO wurtzite crystalline structure. Also, the oxidation states of 2^+ and 3^+ for Fe atoms and 2^+ for Co ones are confirmed. Furthermore, the presence of oxygen vacancies is predicted by EDAX and XAFS. These results, in combination with previous ones, will contribute to the comprehension of the controversial ferromagnetic behavior in these diluted semiconductor materials.

1. Introduction

ZnO is a wide bandgap (E_g = 3.37 eV) semiconductor which presents interesting optical, electronic and magnetic properties that make it a versatile material for a variety of applications. Its large exciton binding energy (60 meV) and non-toxicity are just some of the reasons that have driven research in the last years towards the study of this semiconductor. Moreover, it is known that doping with different metals can improve or modify its promising properties [1,2]. In this sense, the addition of Cd and Mg metals modifies ZnO bandgap [3–5]; trivalent metal doping such as Al, In, Ga, etc. introduces donor levels into the prohibit bandgap, which have different effects in its electronic and optical properties [6–9]. During the last decade, the so-called diluted magnetic semiconductors (DMS) [10] became the most promising studied materials, not only due to their broad application fields (integration of photonic, electronic and magnetic devices) but also because of bandgap tunability. So, the addition of small quantities of magnetic atoms (Mn, Co, Fe and Ni) to ZnO makes this semiconductor an attractive, adequate and cheap material for spintronic applications [11–15]. However, semiconductor doping is not a trivial task although a great variety of methods have been applied; yielding successful results only in some occasions. Techniques such as electrodeposition [16,17], pulsed laser deposition (PLD) [18,19], radiofrequency magnetron sputtering [20–22], different chemical routes [23,24], electron beam evaporation, implantation [25], spray pyrolysis [9,13] and recently, mechanical alloying [6,14,26,27] have been applied to obtain ZnO films and powders with different dopants.

It is known that mechanical alloying or ball milling process can induce chemical reactions in a variety of powder mixtures at low temperature, producing frequently unique and metastable materials that cannot be prepared by conventional techniques [28,29].

This versatile technique was previously applied to obtain Co-doped ZnO [27] and Fe-doped ZnO [6,12,26,30,31] where their structural and magnetic properties were analyzed.

Fe atom is a particular dopant since it presents two different oxidation states which allow us to vary the starting materials: Fe_2O_3, α — Fe or FeO, while Co is isovalent to Zn. In previous works [27,31], magnetic character samples were investigated by measurements in a Quantum Design MPMS-5S superconducting quantum interference device (SQUID) magnetometer. These preliminary results showed no ferromagnetic behaviour at room temperature for both dopants. For the Fe-doped ZnO, we studied the influence of different preparation conditions, such as initial concentrations, atmosphere and milling times on final products by Mössbauer spectroscopy [31,32]. These results indicated that ternary oxides $Zn_{1-x}Fe_xO$ with wurtzite structure are obtained when the precursor oxide is FeO and Fe metal. Instead, when the doping agent is Fe_2O_3 and the milling is done under air atmosphere, a spinel compound is obtained. Mössbauer confirmed that no magnetic structures were present on the final products.

In order to verify the dopant incorporation into the wurtzite ZnO crystalline structure with milling time, an EXAFS (extended X-ray absorption fine structure) and XANES (X-ray absorption near edge spectroscopy), characterization of polycrystalline Co and Fe-doped ZnO oxide is presented in this work. The results are discussed taking into account previous and new magnetic studies on these systems.

* Corresponding author at: Facultad de Ciencias Exactas, Departamento de Física, Universidad Nacional de La Plata (UNLP), CC 67, 1900 La Plata, Argentina. Tel.: +54 221 424 6062; fax: +54 221 425 2006.
E-mail addresses: meyer@fisica.unlp.edu.ar, marcosmey@gmil.com (M. Meyer).

http://dx.doi.org/10.1016/j.powtec.2015.07.006
0032-5910/

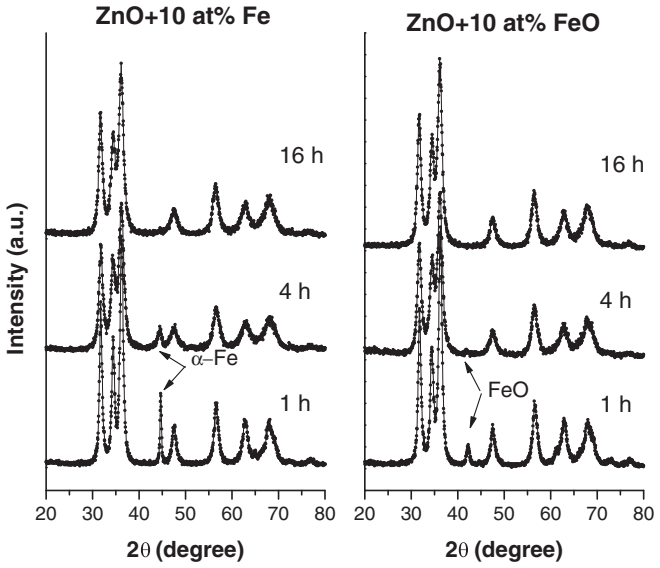

Fig. 1. X-ray diffraction patterns for ZnO + 10% Fe (left) and ZnO + 10% FeO (right) as a function of milling time.

2. Experimental

Several bulk samples were prepared by mechanical milling of ZnO with different percentages (5, 10 and 30 at%) of α — Fe, FeO, Fe_2O_3 and CoO in cylindrical steel milling chamber with one steel ball (diameter: 12 mm). Ball-to-sample mass ratio was 11.5:1. Milling was performed using a horizontal oscillatory mill Retsch at a fixed oscillation frequency of 32 Hz. Powders used were ZnO (Alfa Aesar, Johnson Matthey Co., 99.99), α — Fe (Merk, purity: 99.5), FeO (Sigma Aldrich, purity: 99.9, −10 mesh), Fe_2O_3 (Johnson Matthey Co., purity: 99.99, −15 mesh), CoO (Sigma Aldrich, purity: 99,95, −325 mesh). The Fe-doped samples were handled in a controlled atmosphere chamber (O_2 content less than a few ppm) and milling was conducted in Ar atmosphere.

The obtained powders were characterized by X-ray diffraction (XRD) using a Philips PW 1710 with Cu K_α radiation in the $20° \le 2\theta \le 80°$ range at 0.02°/s.

XAFS measurements were made at RT in transmission mode at the Fe, Co and Zn K-edges using a Si(111) monochromator at the XAFS2 beamline of LNLS (Campinas, Brasil). XAFS analysis was carried out using the IFFEFIT software package with the Athena implementation. Fitting was carried out using the FEFF7 phase and amplitudes. The ATOMS code was used as a tool to generate the input files for FEFF7 based on the ZnO, CoO and iron oxides crystallography data.

The magnetic properties of the samples were measured by a Quantum Design MPMS-5S superconducting quantum interference device (SQUID) magnetometer at different temperatures.

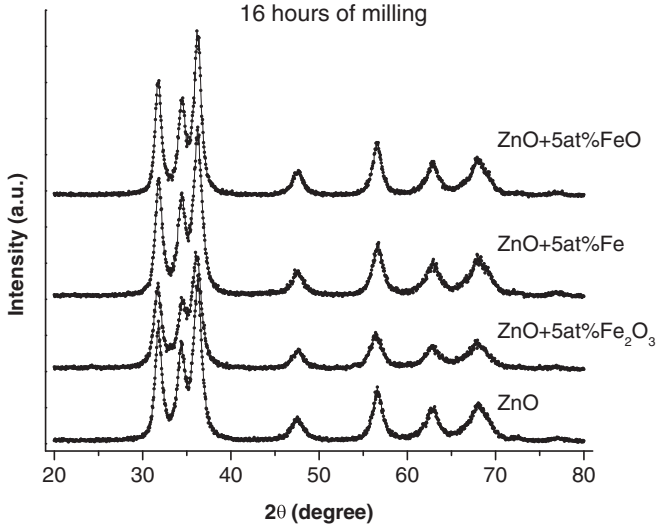

Fig. 2. X-ray diffraction patterns for pure ZnO and −ZnO + 5% (Fe, FeO and Fe_2O_3) after 16 h of milling.

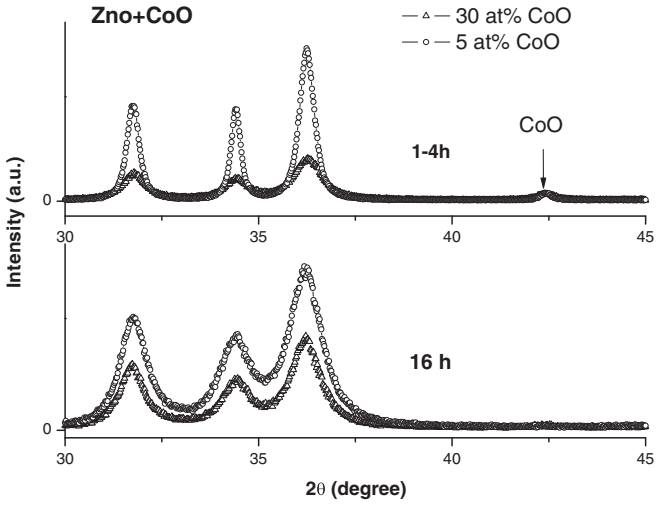

Fig. 3. X-ray diffraction patterns for Co-doped ZnO for different Co content and different milling times.

3. Results and discussion

3.1. XRD

X-ray diffraction patterns displayed similar features for all doped samples and even for the different studied compositions. With increasing milling time, progressive disappearance of characteristic diffraction peak of starting materials, α-Fe, FeO, Fe_2O_3 (Figs. 1 and 2) and CoO (Fig. 3) were observed.

Fig. 1 shows, as an example, the diffraction patterns for ZnO + 10 at% Fe and ZnO + 10 at% FeO obtained at different milling times. It can be seen that diffraction peaks corresponding to α-Fe, FeO were still present after the 4-h milling step. The whole samples, after 16 h of milling, displayed only the ZnO structure diffraction peaks (P63 mc) (Fig. 2) [32]. Similar features were observed for the case of CoO. In Fig. 3, the diffraction patterns corresponding to ZnO + 5 at% CoO and ZnO + 30 at% CoO at milling times of 1 and 4 h (upper) and 16 h (bottom) of milling are shown. After the final milling step, no traces of CoO were seen.

As milling proceeds, a peak broadening, associated to a decrease in grain size, was observed for all the studied samples. Rietveld refinement allowed us to estimate final crystallite sizes at about 20 nm [27,32,33]. Table 1 shows values for crystallite size and microstrain, obtained using the Williamson–Hall model for Fe-doped samples [27–32].

Table 1
Crystallite size and microstrain, obtained using the Williamson–Hall model for 10 at% Fe-doped samples after 16 h of milling.

Sample	Phase	Size (nm)	Strain($x10^{-3}$)
ZnO + Fe_2O_3	$ZnFe_2O_4$	51_3	0.30_2
	ZnO	38_3	0.52_2
ZnO + FeO	ZnO	22_2	0.46_1
ZnO + Fe	ZnO	19_1	0.32_1

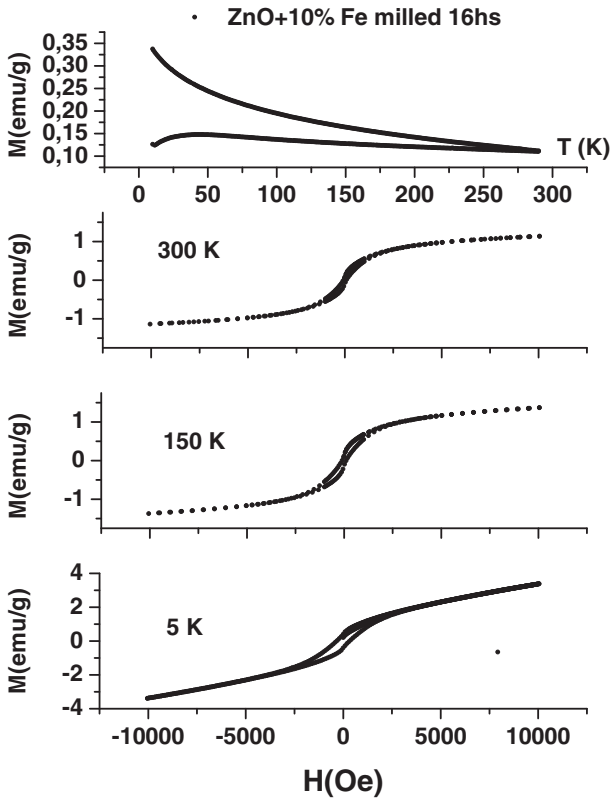

Fig. 4. Magnetic measurements of ZnO + 10 at% Fe milled 16 h. ZFC FC and magnetization in function on applied field.

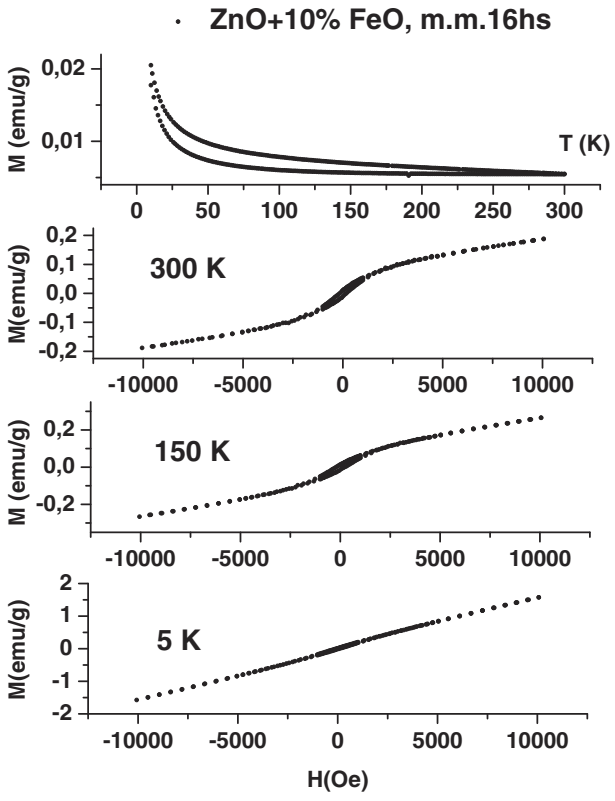

Fig. 5. Magnetic measurements of ZnO + 10 at% FeO milled 16 h. ZFC FC and magnetization in function on applied field.

3.2. Magnetic measurements

The influence of milling time on magnetic properties was studied in these alloys. Samples containing ZnO + 10 at% Fe and ZnO + 10 at% FeO were investigated. The magnetization curves at different temperatures for 16 h milled 10 at% Fe-doped sample at a maximum applied field of 10 kOe are shown in Fig. 4 together with zero field cooling-field cooling (ZFC-FC) curves. The ZFC-FC curves were obtained cooling the sample from RT up to 5 K without an applied magnetic field. Then, an external magnetic field was turned on while the temperature of the sample was increased until it reached RT. Finally, keeping the applied external magnetic field the temperature was diminished to 5 K. The ferromagnetic contribution, due to Fe, decreased with milling time while the paramagnetic contribution became more important. This fact is consistent with X-ray diffraction results where a progressive incorporation of Fe into the wurzite-type crystalline structure with milling time was observed. The blocking temperature, associated with the maxima at the warming part of the curve, was shifted to lower values with increasing milling time. In this case, it can be observed that this blocking temperature was near 40 K for the sample milled for 16 h.

Fig. 5 displays the measurements of the sample containing 10 at% FeO milled 16 h. The magnetization curves show a paramagnetic

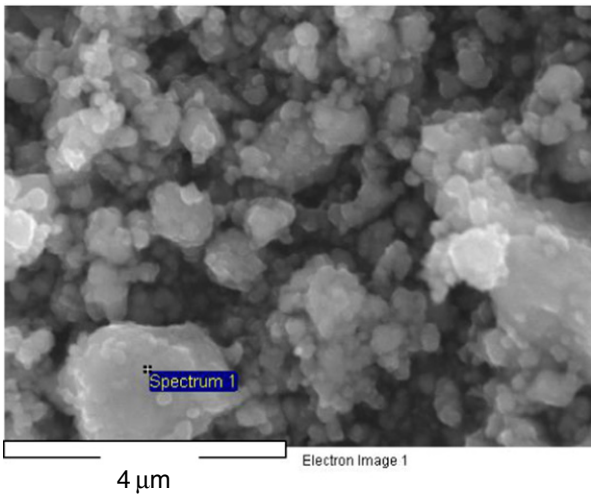

a) ZnO + 10% FeO, milled 16 h

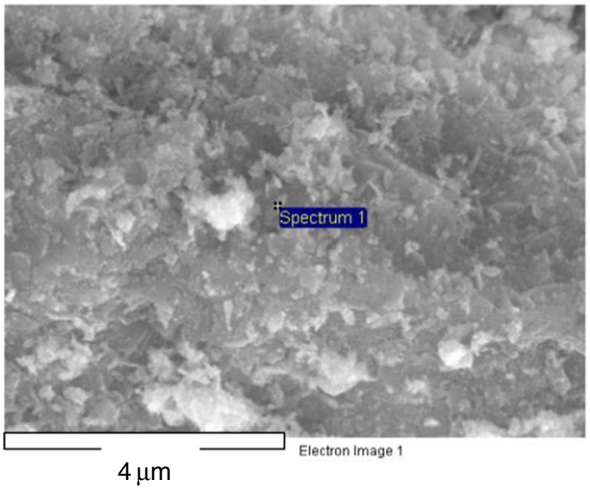

b) ZnO + 10% Fe_2O_3, milled 16 h

Fig. 6. SEM images for ZnO milled 16 h doped with (a) 10% Fe_2O_3 milled in air and (b) 10% FeO.

Table 2
Atomic percent compositions of the constituents of three of the doped ZnO nanoparticles obtained from EDAX as milling time increase. The last column shows the Zn and doped atom to oxygen ratios.

Sample	Milling Time (h)	Element	at.%	Zn-Doped Atom/O Ratio
ZnO + 30% CoO	1	Zn	32.41	1.10
		Co	17.93	
		O	45.66	
	2	Zn	48.94	3.04
		Co	26.31	
		O	24.7	
	16	Zn	34.3	1.25
		Co	21.3	
		O	44.5	
ZnO + 10% FeO	1	Zn	44.45	0.91
		Fe	3.14	
		O	52.34	
	4	Zn	31.27	0.72
		Fe	15.91	
		O	65.67	
	16	Zn	32.81	0.56
		Fe	3.02	
		O	64.17	
ZnO + 10% Fe_2O_3	1	Zn	14.98	0.39
		Fe	13.11	
		O	71.91	
	4	Zn	25.22	0.49
		Fe	7.57	
		O	67.21	
	16	Zn	28.31	0.54
		Fe	6.71	
		O	64.98	

behavior with a small ferromagnetic contribution at 150 K and 300 K and proportionally very weak one at 5 K. No saturation was achieved in the full studied magnetic field range and no blocking temperature was observed. The ferromagnetic contribution is one order of magnitude lower than the sample containing 10 at% Fe. Similar behavior was observed in samples prepared with Co, indicating a substitution of Co in the Zn sites as milling proceeds (not shown) [27]. No blocking temperature was observed for samples doped with 5 at% of Co.

After 16 h of milling for the whole samples, the loops were described with two contributions, (i) a paramagnetic component dominating even at 5 K, responsible for the straight tails at high field in all samples at all temperatures, and (ii) a second very weak ferromagnetic, practically independent from temperature, incompatible with superparamagnetic particles, suggesting a long-range coupling between magnetic moments.

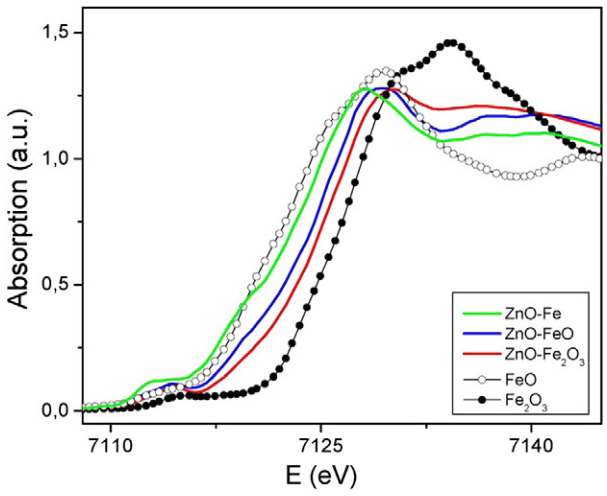

Fig. 7. Fe K-edge XANES spectra of ZnO + 10% (Fe, FeO and Fe_2O_3) samples. FeO and Fe_2O_3 reference material for Fe^{2+} and Fe^{3+}, respectively, are also shown.

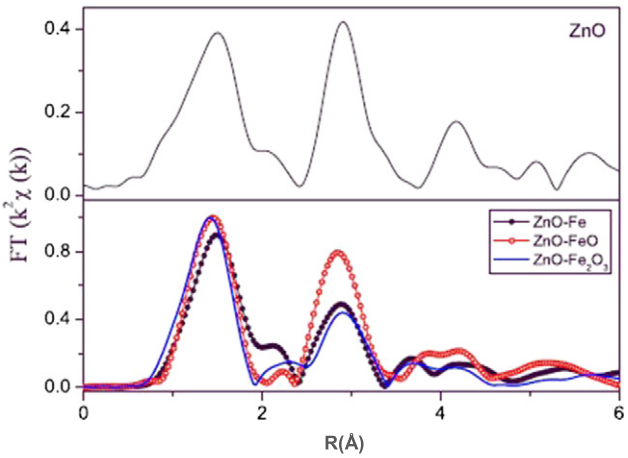

Fig. 8. Fourier transform intensities for the Fe-, FeO- and Fe_2O_3-doped ZnO samples milled 16 h compared with the ZnO reference.

These results agreed with previous Mössbauer studies [31,32] where different paramagnetic and magnetic signals were observed.

3.3. SEM

The microstructure of the different samples was analyzed by SEM. Grain size reduction and homogenization were achieved for prolonged milling times in all cases. Fig. 6 shows SEM images at different milling times for mixtures of hematite (milled in air) and α-Fe. In the former case, a spinel structure was formed [32] with a different final morphology (Fig. 6a) Similar microstructure to 10% FeO-doped sample (Fig. 6b) after 16 h of milling were obtained for the other doped samples.

The atomic percent compositions (say at%) of the constituents of three of the doped ZnO nanoparticles obtained from EDAX as milling time increases are summarized in Table 2. For the case of Co-doped samples (30 at%), the Zn-Co/O ratio at% is 55.6/44.5, close to the expected ratio for the semiconductor ZnO. Instead, for the iron-doped samples, an excess of oxygen in the ZnO nanoparticles was obtained which could be attributed to interstitial oxygen (O_i) in the nanoparticles [34].

3.4. XAFS

With the aim to verify the incorporation of doping atom into the host semiconductor, XAFS measurements were done on the studied samples.

In Fig. 7, the Fe K-edge XANES spectra of ZnO + 5 at% (Fe, FeO, Fe_2O_3) 16 h milled samples are shown. Spectra of FeO and Fe_2O_3 as reference materials are also included for comparison purposes. The studied samples have energy edges between those of FeO and Fe_2O_3, indicating a mixture of Fe^{2+} and Fe^{3+} oxidation states.

Table 3
Fitting results of the first, second and third shell of neighboring atoms around the Fe one compared with ZnO reference ones. *NN* is the number of atoms located at a distance *R* from the central atom and σ^2 is the Debye–Waller factor.

Sample		*NN*	*R* (Å)	σ^2 (Å^2)
ZnO	O	4	1.97_2	0.009_1
	Zn	6	3.20_9	–
	O	6	3.24_9	–
ZnO-Fe	Fe-O	3.4_2	1.97_4	0.006_2
	Fe-$Fe_{(8)}$	1.9_5	2.48_1	0.018_4
	Fe-$Zn_{(12)}$	7.8_7	3.25_2	0.021_2
ZnO-FeO	Fe-O	3.2_3	1.95_4	0.005_2
	Fe-$Zn_{(12)}$	9.8_5	3.25_5	0.009_3
ZnO-Fe_2O_3	Fe-O	3.1_4	1.94_3	0.008_3
	Fe-$Fe_{(4)}$	1.9_2	3.01_4	0.014_4
	Fe-$Zn_{(12)}$	8.3_5	3.23_2	0.023_5

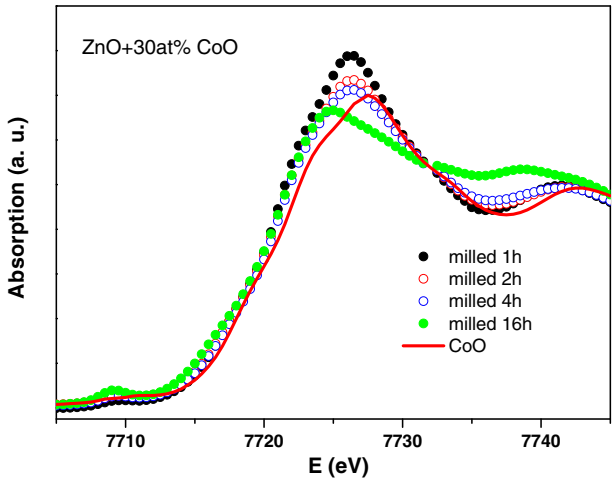

Fig. 9. Co K-edge XANES spectra of ZnO + 30% CoO samples at different milling times. CoO reference material for Co^{2+} is also shown.

The Fourier transformed (FT) of $k^2\chi(k)$ data in the range 2 to 11 $Å^{-1}$ are shown in Fig. 8 together with that of ZnO measured at the Zn K-edge. The doped samples display a very similar feature to that of pure ZnO. Both undoped and doped ZnO Fourier transforms are consistent with results obtained by other authors [35] for ZnO nanoparticles of 70 nm mean diameter and simulations on bulk ZnO [36].

The changes in structural parameters arising from different starting materials were analyzed by fitting the first two peaks in the Fourier transform. The obtained fitted parameters are reported in Table 3. It was proposed to fit with three layers (Fe-O, Fe-Fe and Fe-Zn) in the case of Fe- and Fe_2O_3-doped samples and with two layers for the FeO-doped samples (Fe-O and Fe-Zn).

In all samples, the first oxygen shell coordination number was smaller than the corresponding Zn in ZnO, indicating the presence of oxygen vacancies. The metallic Fe-doped sample displays a Fe neighbor second layer at a distance (R) similar to the corresponding one in bcc-Fe. Also, R values for the third layers of Zn neighbors remained similar to those of Zn in ZnO, but its coordination number was smaller. The σ^2 values of the Fe-Fe and Fe-Zn pairs in the ZnO-Fe and ZnO-Fe_2O_3 samples were about two to three times larger than that of ZnO-FeO powder. These features confirmed the presence of significant structural disorder in the Fe–Zn pairs of these samples.

These results suggest a good agreement in distance and coordination number as expected for Fe replacing Zn in ZnO.

Co-K edge XANES spectra for ZnO + 30% CoO milled samples were obtained. In all of them, energy positions of the edge coincided with the CoO one, indicating that Co ions exhibit a 2^+ oxidation state (Fig. 9). The Fourier transformed (FT) XAFS data of samples at different milling times together with CoO one for comparison purposes are shown in Fig. 9. Samples milled 1, 2 and 4 h present FT with a similar CoO structure, considering peak positions, but with decreasing intensities with milling time (see Fig. 10a).

Fig. 10b shows the data for the last two milling steps. The first peak corresponds to Co-O coordination while the second one is associated with Co-Co coordination. As milling time increases, their relative intensities change and the third peak is shifted to higher distances.

In order to analyze these changes in the structural parameters, the first and second peak of FT was back-transformed and fitted with two layers for samples milled for 1, 2 and 4 h, and with three layers for samples milled for 8 and 16 h. The obtained fitted parameters are reported in Table 4 and the XAFS oscillation data overlaid with the fit curve corresponding to the 16-h milled sample is displayed in Fig. 11. From these results, it can be seen that oxygen coordination decreased from 6 (expected for the CoO phase) to 3.5 Å (likely Zn in ZnO structure). After 16 h of milling, Co-Co coordination diminished progressively from 12 to 2.9 and a new contribution of Zn at 3.25 Å arose after 8 h of milling. This new Co-Zn layer has coordination number and distance similar to those expected for Co substituting Zn in wurtzite structure.

Moreover, the σ^2 value of the Co–O pairs decreases as milling time increases, suggesting a kind of structural order in the system.

4. Conclusions

In the whole ZnO-doped samples, mechanical milling leads to almost total cation substitution in the wurtzite ZnO structure as

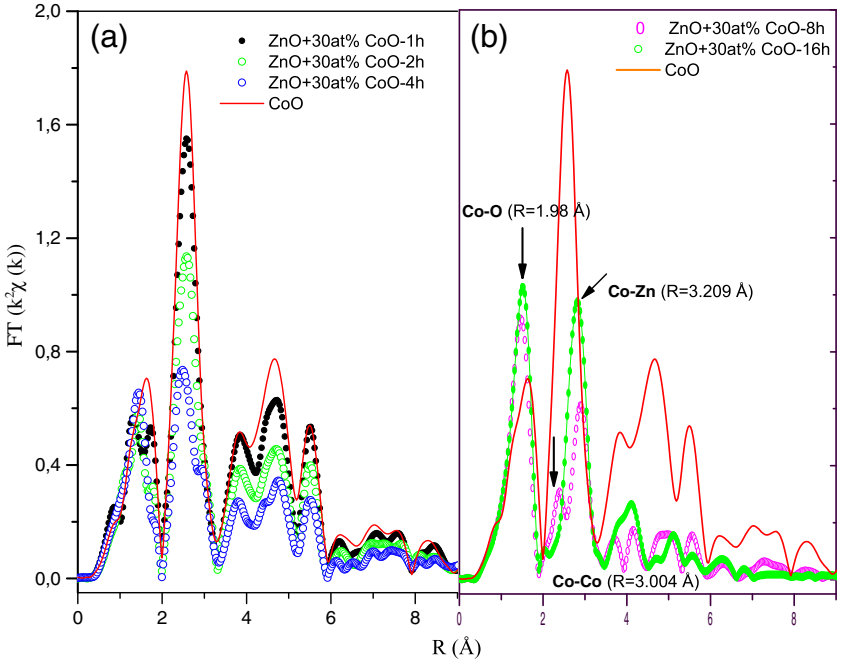

Fig. 10. Fourier transform intensities for (a) the Co-doped ZnO samples milled 1, 2 and 4 h compared with CoO reference, (b) the Co-doped ZnO samples milled 8 and 16 h compared with CoO and ZnO references.

Table 4
Fitting results of the first, second and third shell of neighboring atoms around the Co one compared with ZnO reference ones. *N* is the number of atoms located at a distance *R* from the central atom and σ^2 is the Debye–Waller factor.

Sample		*NN*	*R* (Å)	σ^2(Å^2)
ZnO (ref.)	O	4	1.97_1	0.009_1
	Zn	6	3.20_9	–
	O	6	3.24_9	–
CoO	O	6	2.10_2	0.015_3
	Co	12	3.00_1	0.009_1
1 h	O	5.8_2	2.07_2	0.015_3
	Co	10.5_3	2.99_1	0.009_1
2 h	O	5.3_3	2.03_2	0.015_3
	Co	7.9_2	2.99_1	0.009_1
4 h	O	5.0_2	2.01_1	0.015_3
	Co	4.9_2	2.97_1	0.009_1
8 h	O	3.6_1	1.97_2	0.004_2
	Co	3.2_4	2.95_3	0.009_1
	Zn	4.0_1	3.25_1	0.010_1
16 h	O	3.5_1	1.97_1	0.004_2
	Co	2.9_3	2.90_2	0.009_1
	Zn	5.0_1	3.25_1	0.010_1

confirmed by X-ray diffraction. From the local structure investigation by means of XAFS technique, the oxidation state of cation atoms could be obtained. From these results, the iron ions are in 2^+ and 3^+ oxidation states while Co atoms are in 2^+ oxidation state. As a consequence, it can be concluded that Fe and Co are preferentially substituting Zn in ZnO structure. EXAFS analysis also indicated the presence of oxygen vacancy around iron substituting the Zn ions, in agreement with EDAX results. The magnetic measurements indicate that two magnetic phases are present, a ferromagnetic phase and a paramagnetic phase. The relative ferromagnetic contribution phase becomes more important at high temperatures.

The present SQUID measurements cannot be explained only in terms of Fe oxidation states. Samples with oxidation state near to +2 (ZnO + 10 at% Fe) have a ferromagnetic component with a saturation magnetization one order of magnitude higher than samples with oxidation states between +2 and +3 (ZnO + 10 at% FeO). This difference cannot be justified by considering Hund's rules and the different oxidation states to determine the magnetic moment of Fe atoms.

The SQUID measurements are consistent with an electronic configuration strongly influenced by crystalline field. In this sense, one possibility would be that Fe + 2 has a high spin configuration and Fe + 3 a lower one.

Acknowledgements

This work was supported by Consejo Nacional de Investigaciones Científicas y Técnicas (CONICET) and Fac. Cs. Exactas (UNLP).

References

[1] S.J. Pearton, D.P. Norton, K. Ip, Y.W. Heo, T. Steiner, Recent progress in processing and properties of ZnO, Prog. Mater. Sci. 50 (2005) 293–340.
[2] M.D. McCluskey, S.J. Jokela, Defects in ZnO, J. Appl. Phys. 106 (2009) 071101, http://dx.doi.org/10.1063/1.3216464.
[3] Fazhan Wang, Zhizhen Ye, Dewei Ma, Liping Zhu, Fei Zhuge, Formation of quasi-aligned ZnCdO nanorods and nanoneedles, J. Cryst. Growth 283 (2005) 373–377.
[4] Deuk-Kyu Hwang, Min-Chang Jeong, Jae-Min Myoung, Effects of deposition temperature on the properties of $Zn_{1-x}Mg_xO$ thin films, Appl. Surf. Sci. 225 (2004) 217–222.
[5] T. Makino, A. Ohtomo, C.H. Chia, Y. Segawa, H. Koinuma, M. Kawasaki, Internal electric field effect on luminescence properties of ZnO/(Mg, Zn)O quantum wells, Phys. E. 21 (2004) 671–675.
[6] L.C. Damonte, V. Donderis, M.A. Hernández-Fenollosa, Trivalent dopants on ZnO semiconductor obtained by mechanical milling, J. Alloys Compd. 26 (Issues 1–2) (2009) 442–444, http://dx.doi.org/10.1016/j.jallcom.2008.07.216.
[7] Junjun Jia, Aiko Takasaki, Nobuto Oka, Yuzo Shigesato, Experimental observation on the Fermi level shift in polycrystalline Al-doped ZnO films, J. Appl. Phys. 112 (2012) 013718, http://dx.doi.org/10.1063/1.4733969.
[8] Anita Vandna Luthra, Tweaking electrical and magnetic properties of Al–Ni co-doped ZnO nanopowders, Ceram. Int. 40 (2014) 14927–14932.
[9] A. Amala Rani, Suhashini Ernest, Structural, morphological, optical and compositional characterization of spray deposited Ga doped ZnO thin film for dye-sensitized solar cell application, Superlattice. Microst. 75 (2014) 398–408.
[10] Tomasz Dietl, A ten-year perspective on dilute magnetic semiconductors and oxides, Nat. Mater. 9 (2010) 965–974, http://dx.doi.org/10.1038/nmat2898.
[11] Y.Q. Wang, S.L. Yuan, L. Liu, P. Li, X.X. Lan, Z.M. Tian, J.H. He, S.Y. Yin, Ferromagnetism in Fe- doped ZnO bulk samples, J. Magn. Magn. Mater. (2007) 1423–1426, http://dx.doi.org/10.1016/j.jmmm.2007.10.007.
[12] Y. Lin, D. Jiang, F. Lin, W. Shi, X. Ma, Fe-doped ZnO magnetic semiconductor by mechanical alloying, J. Alloys Compd. 436 (Issues 1–2, 14) (2007) 30–33.
[13] Said Benramache, Boubaker Benhaoua, Okba Belahssen, The crystalline structure, conductivity and optical properties of Co-doped ZnO thin films, Optik 125 (2014) 5864–5868.
[14] Katsuhisa Tanaka, Kazuya Fukui, Shunsuke Murai, Koji Fujita, Mechanical milling-induced room-temperature ferromagnetic phase in MnO_2–ZnO system, Appl. Phys. Lett. 89 (2006) 052501, http://dx.doi.org/10.1063/1.2234269.
[15] Faheem Ahmed, Shalendra Kumar, Nishat Arshi, M.S. Anwar, Si Nae Heo, Bon Heun Koo, Direct relationship between lattice volume, bandgap morphology and magnetization of transition metals (Cr, Mn and Fe)-doped ZnO nanostructures, Acta Mater. 60 (2012) 5190–5196.
[16] B. Marí, A. Elmanouni, L.C. Damonte, M. Mollar, Preparation and characterization of Zn1-xFexO thin films, Phys. Status Solidi A 207 (2010) 1623–1626.

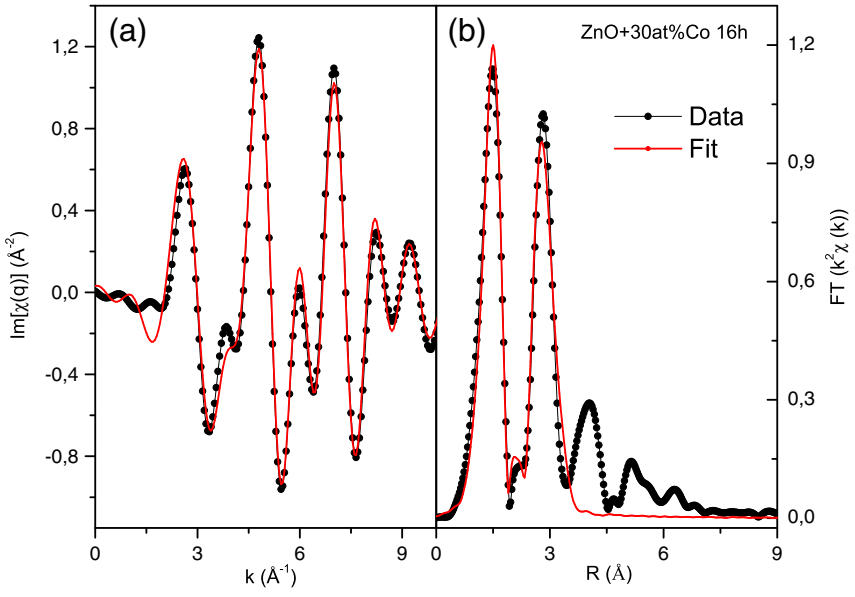

Fig. 11. (a) k^2 weighted EXAFS with fit for ZnO + 30 at% CoO and (b) corresponding Fourier transforms with fit for ZnO + 30 at% CoO sample milled 16 h.

[17] V. Donderis, J. Orozco, J. Cembrero, J. Curiel-Esparza, L.C. Damonte, M.A. Hernández-Fenollosa, Doped nanostructured zinc oxide films grown by electrodeposition, J. Nanosci. Nanotechnol. 10 (2010) 1387–1392.
[18] J.A. Sans, A. Segura, J.F. Sánchez-Royo, V. Barber, M.A. Hernández-Fenollosa, B. Marí, Correlation between optical and transport properties of Ga-doped ZnO thin films prepared by pulsed laser deposition, Superlattice. Microst. 39 (2006) 282–290.
[19] Wenda Zhao, Qianfei Zhou, Xin Zhang, Xiaojing Wu, A study on Ti-doped ZnO transparent conducting thin films fabricated by pulsed laser deposition, Appl. Surf. Sci. 305 (2014) 481–486.
[20] D.P. Xiong, X.G. Tang, W.R. Zhao, Q.X. Liu, Y.H. Wang, S.L. Zhou, Deposition of ZnO and MgZnO films by magnetron sputtering, Vacuum 89 (2013) 254–256.
[21] Junjun Jia, Aiko Takasaki, Nobuto Oka, Yuzo Shigesato, Experimental observation on the Fermi level shift in polycrystalline Al-doped ZnO films, J. Appl. Phys. 112 (2012) 013718, http://dx.doi.org/10.1063/1.4733969.
[22] Anil Singh, Sujeet Chaudhary, Dinesh K. Pandya, On the temperature dependence of mobility in hydrogenated indium-doped ZnO thin films, Acta Mater. 77 (2014) 125–132.
[23] Thomas Verdier, Virginie Nachbaur, Malick Jean, Mechanosynthesis of zinc ferrite in hardened steel vials: Influence of ZnO on the appearance of Fe(II), J. Solid State Chem. 178 (2005) 3243–3250.
[24] C.-W. Chang, H.-T. Wu, S.-H. Huang, C.-K. Chen, I.-W. Un, T.-J. Yen, Single-crystalline heterostructure of ZnO nanowire arrays on large Ag microplates and its photocatalytic activity, Acta Mater. 61 (2013) 6993–6999.
[25] I.P. Keßler, K. Lorenz, R. Vianden, Implanted impurities in wide band gap semiconductors, Defects Diffusion Forum, 38, Trans Tech Publications 2011, pp. 167–179.
[26] S. Karamat, R.S. Rawat, P. Lee, T.L. Tan, R.V. Ramanujan, Structural, elemental, optical and magnetic study of Fe doped ZnO and impurity phase formation, Prog. Nat. Sci.: Mater. Int. 24 (2014) 142–149.
[27] L.C. Damonte, M.A. Hernández-Fenollosa, M. Meyer, L. Mendoza-Zélis, B. Marí, Structural and magnetic properties in mechanically alloyed $Zn_{1-x}Co_xO$ semiconductor powders, Physica B 398 (2) (2007) 380–386.
[28] C. Suryanarayana, Mechanical alloying and milling, Prog. Mater. Sci. 46 (2001) 1–184.
[29] L. Takacs, Self-sustaining reactions induced by ball milling, Prog. Mater. Sci. 47 (2002) 355–414.
[30] L. Baum, M. Meyer, D. Richard, L.C. Damonte, L.A. Mendoza-Zélis, Mossbauer characterization of Fe-doped ZnO prepared by mechanical milling, Hyperfine Interact. 176 (2007) 87–92.
[31] L. Damonte, M. Meyer, L. Mendoza Zélis, Mechanical dopping of ZnO powders, J. Alloys Compd. 536 (2012) S495–S498.
[32] L.C. Damonte, M. Meyer, L. Baum, L. Mendoza Zélis, Mössbauer study on $Zn_{1-x}Fe_xO$ semiconductors prepared by high energy ball milling, Hyperfine Interact. 195 (2010) 227–233.
[33] L.C. Damonte, L.A. Mendoza Zélis, B. Marí Soucase, M.A. Hernández Fenollosa, Nanoparticles of ZnO obtained by mechanical milling, Powder Technol., 148, Elsevier Science 2004, pp. 15–19.
[34] J. Timoshenko, A. Anspoks, A. Kalinko, A. Kuzmin, Temperature dependence of the local structure and lattice dynamics of wurtzite-type ZnO, Acta Mater. 79 (2014) 194–202.
[35] Eun-Suk Jeong, Hyo-Jong Yu, Yong-Jin Kim, Gyu-Chul Yi, Yong-Dae Choi, Sang-Wook Han, Local structural and optical properties of ZnO nanoparticles, J. Nanosci. Nanotechnol. (2010) 3562–3565.
[36] Anshuman Sahai, Navendu Goswami, Probing the dominance of interstitial oxygen defects in ZnO nanoparticles through structural and optical characterizations, Ceram. Int. 40 (2014) 14569–14578.